1.1.2 Thermal blooming of high-power laser beams

The longitudinal scale of variability for thermal inhomogeneities induced in the propagation channel of a high-power laser beam is comparable to the diffraction length of the beam. In the interval Δz, the equation for the phase screen can be approximated by the product of a step length Δz and the refractive index distribution at the center of the interval $[z_l; z_l+\Delta z]$:

$$\varphi_l(\vec{\rho}) = k\Delta z \delta n\left(\vec{\rho}, z_l + \frac{1}{2}\Delta z\right) + O(\Delta z^2)\,. \tag{1.1.13}$$

It follows from the above that we have only to determine perturbations of the refractive index in some planes, the positions of which are determined by the scheme of the splitting algorithm.

Heating of the medium that is caused by absorption of radiation energy induces variation of its density, which leads to a decrease in the refractive index related to the density ρ by the following law [26]:

$$\delta n = K\rho\,, \tag{1.1.14}$$

where K is a constant equal to two-thirds of the polarization factor of a molecule or gas atom.

In the isobaric approximation, the density of the medium is explicitly related to temperature by the ideal gas law, so variations of the refractive index can be expressed through temperature variations:

$$\delta n \approx \frac{\partial n}{\partial T}(T - T_0) = n'_T \delta T. \tag{1.1.15}$$

The isobaric approximation is valid for the normal atmospheric conditions. Exceptions are fast scanning of a continuous-wave (cw) high-power beam when the beam speed with respect to the medium is greater than the sonic speed, and when the pulse duration τ_p is comparable with the acoustic time τ_s:

$$\tau_p = \tau_S = a / c_S\,, \tag{1.1.16}$$

where a is the beam size and c_s is the sonic speed.

When the isobaric approximation is valid, the distribution of the refractive index in the beam cross section is determined by the heat balance, which is described by the heat transfer equation for the temperature field $T(x, y, z)$:

$$\frac{\partial T(x,y,z)}{\partial t} + \vec{V}_\perp \nabla T - \chi \Delta_\perp T = \frac{\alpha}{\rho_0 C_p} I, \tag{1.1.17}$$

where $\vec{V}_\perp = (V_x, V_y)$ is the transverse component of the beam velocity relative to the medium, χ is heat conductivity, ρ_0 is the specific density of the medium, α is the absorption coefficient, and C_p is the specific heat at constant.

When the isobaric approximation becomes invalid, variations in the density of the medium are described by the linearized equations of hydrodynamics, which follow from the law of continuity and the laws of impetus and energy conservation [21, 26]:

$$\frac{d\rho_1}{dt} + \rho_0 \nabla v_1 = 0, \qquad \frac{d}{dt} = \frac{\partial}{\partial t} + v_0 \frac{\partial}{\partial x}, \tag{1.1.18}$$

$$\rho_0 \frac{dv_1}{dt} = -\nabla p_1, \tag{1.1.19}$$

$$\frac{d}{dt}(p_1 - c_S^2 \rho_1) = (\gamma - 1)\alpha I. \tag{1.1.20}$$

These equations are valid for small perturbations of density ρ_1, pressure p_1, and local speed of the medium flow v_1 with respect to the unperturbed values of density ρ_0, pressure p_0, and local speed of medium flow v_0 along the x-axis. By eliminating the variables describing perturbation of speed and pressure, Eqs. (1.1.18)–(1.1.20) can be transformed into the following equation, which describes perturbations of the density:

$$\left(\frac{d^2}{dt^2} - c_S^2 \nabla^2 \right) \frac{d\rho_1}{dt} = (\gamma - 1)\alpha \nabla^2 I. \tag{1.1.21}$$

For a steady-state condition, this equation takes the form

$$\left[\frac{\partial^2}{\partial y^2} + (1 - M^2) \frac{\partial^2}{\partial x^2} \right] \frac{d\rho_1}{dx} = \frac{(\gamma - 1)}{c_S^2 v} \alpha \nabla^2 I, \tag{1.1.22}$$

where $M = v / c_S$ is Mach's number and $\gamma = C_p/C_v$ is the specific heat ratio at a constant volume.

When the flow rate of the medium is low ($M = v / c_S << 1$), Eq. (1.1.22) transforms into the equation written in the isobaric approximation:

$$\frac{d\rho_1}{dx} = \frac{(\gamma - 1)}{c_S^2 v} \alpha I. \tag{1.1.23}$$

Solution of this equation yields a result equivalent to that of Eq. (1.1.17), with $v_y = 0$ and $\chi = 0$.

With no wind, under *conditions of gravitational convection*, the heat balance equation should be solved by a set of equations for incompressible liquid hydrodynamics. The plane (2D) flow of this liquid in the Boussinesq–Oberbeck approximation is described by the vortex (vorticity) function ω and the stream function ψ [27] equations:

$$\frac{\partial \omega}{\partial t} + \vec{v}\vec{\nabla}_{\perp}\omega = \nu\Delta_{\perp}\omega + \beta g\frac{\partial T}{\partial x} \ ; \tag{1.1.24}$$

$$\Delta_{\perp}\psi = -\omega, \tag{1.1.25}$$

where β is the volume expansion coefficient, ν is the kinematic viscosity coefficient, and g is the absolute value of the acceleration of gravity directed along the 0y axis.

The local speed of the flow in the equations for temperature and vorticity is now a function of transverse coordinates. Its components are related to the partial derivatives of the stream function as follows:

$$v_x = \frac{\partial \psi}{\partial y}, \quad v_y = -\frac{\partial \psi}{\partial x} \ . \tag{1.1.26}$$

When describing thermal blooming under conditions of free convection, Eqs. (1.1.17), (1.1.24), and (1.1.25) are complemented by the corresponding initial and boundary conditions. In the case of propagation in a closed space, they are the conditions of adhesion and zero flow speed at the boundary Γ for the normal and tangential components of the flow velocity:

$$v_n(x,y) = 0, \quad v_s(x,y) = 0, \quad (x,y) \in \Gamma \, . \tag{1.1.27}$$

These conditions in turn determine the boundary conditions for the stream function and its derivative with respect to the normal to the boundary surface:

$$\psi(x,y) = 0, \quad \frac{\partial \psi}{\partial n} = 0, \quad (x,y) \in \Gamma. \tag{1.1.28}$$

The boundary and initial conditions for the temperature field are usually set to be zero.

So the mathematical model of thermal blooming of high-power coherent laser beams in a low-absorbing medium includes the parabolic wave equation for the scalar complex amplitude [Eq. (1.1.4)] and the corresponding material

equation (or set of equations) describing density and temperature variations and determining the distribution of the refractive index in the beam channel:

$$\begin{cases} 2ik\dfrac{\partial E}{\partial z} = \left(\dfrac{\partial^2}{\partial x^2} + \dfrac{\partial^2}{\partial y^2} + 2k^2 \delta n \right) E \\ \hat{M}(\delta n) = \alpha I \end{cases}, \qquad (1.1.29)$$

where the operator $\hat{M}$ describes the relation between the induced optical inhomogeneities and the absorbed energy αI.

Below we present the results of applying our numerical technique for estimating the thermal blooming distortions of coherent beams propagating along atmospheric paths that were developed in Refs. [4], [16-18], [24], [30], and [49]. To allow for the regular altitudinal variation of thermodynamic parameters, we have used statistical seasonal atmospheric models, built from refined data obtained by the Institute of Atmospheric Optics in Tomsk [56-58]. The altitude profile of the molecular absorption coefficient for summer and winter mean-latitude models was obtained by means of a software program that calculates molecular absorption line by line [59].

As an example of implementation of the mathematical model, let us consider the results computed for thermal blooming of a focused Gaussian beam crossing a thin layer L of a nonlinear medium (nonlinear phase screen). In this example, the approximation of a nonlinear phase screen indicates that the thickness L of the layer is much shorter than the beam focal length and the diffraction length $L_d = ka_0^2$ of the beam and that the Bouguer extinction is low ($\alpha L << 1$).

In Fig. 1.1.1, the dynamics of thermal blooming under conditions of forced convection are illustrated for a convective flow speed that is much lower than the sonic speed [isobaric approximation, Eq. (1.1.17)] and for the heat conductivity $\chi = 0$. In this case, the sole parameter of the problem [56-59] is the integral nonlinearity of the medium layer:

$$P_N = \frac{2\pi}{\lambda} \frac{\alpha a_0 I_0}{\rho C_p V_\perp} n_T' L ,$$

where I_0 is the initial intensity of the beam, a_0 is the initial size of the Gaussian beam, and α is the Bouguer extinction of media. When transient processes end, the phase screen can be described as an integral of the normalized beam intensity:

$$\varphi(x,y) = P_N \int_{-\infty}^{x} I(\xi, y) \Big/ I_0 d\xi = P_N \int_{-\infty}^{x} \exp\left(-\xi^2 - y^2\right) d\xi . \qquad (1.1.30)$$

At a large distance x, the value of phase φ at the 0z axis ($y = 0$) tends toward $\sqrt{\pi}P_N \approx 1.77P_N$. In calculations, the value of P_N was assumed to be equal to 10; this value corresponds to the maximal phase difference of 17.7 rad or 2.8λ. For such nonlinear distortions, the steady-state maximal value of the focus intensity decreases more than 10 times. Figure 1.1.1 shows two examples of calculations for different directions of the wind vector. For every instant of time t (here, time t is normalized at a value of $a_0/V_\perp$, where $V_\perp$ is wind velocity) the 2D distributions of phase distortions in the plane of the emitting aperture are shown, along with the intensity distribution in the focal plane for the Gaussian beam. In the first case the wind was directed along the ordinate; and in the second case, the angle between the wind and the ordinate was 45 deg.

Figure 1.1.2 shows typical images of thermal blooming of laser radiation under different stream velocities. The numbers in each image box of Figs. 1.1.1 and 1.1.2 show the maximum and minimum values of the functions $I(\vec{\kappa})$ and $\varphi(\vec{\rho})$. It can be seen that the estimate of phase distortions in the steady state (17.7 rad) is in good agreement with the results obtained in the numerical experiment (16.9 and 16 rad). The difference of 5–10% can be attributed to the error of the numerical model and the fact that the transient processes did not end completely.

The calculations have been performed by the monotonic conservative procedure with the second-order approximation, differences were taken with respect to the stream [27], and the model viscosity (heat conductivity) was compensated for according to Samarskii's algorithm [28]. The advantage of this method is that it makes it possible to solve the dynamic problem of heat transfer at an arbitrary orientation of the wind vector. The method is stable for both small and large intervals of time discretization and it allows the solution of the heat transfer problem when wind velocity depends on the transverse coordinates (x,y). Thus, the calculations can be performed for the problem of thermal blooming under free (gravitational) convection conditions [Eq. (1.1.17) together with Eqs. (1.1.24) and (1.1.25)], as well as the boundary conditions of adhesion and zero speed. Some sample calculations are given in Ref. [29]. In this text we do not consider these convection conditions in greater detail because gravitational convection is atypical for open atmospheric paths.

Next we consider the situation of a high-power beam with scanning. In this case, the speed of beam transition with respect to the medium at some distance from the source can be close to or even higher than sonic speed. In Fig. 1.1.2, density perturbations are shown for forced convection conditions with the speed of the flow close to sonic speed [Eq. (1.1.22)]. The value of the parameter P_N was assumed to be two times smaller than in the previous example. In the isobaric approximation, this corresponds to the maximal phase change on the path (8.8 rad). It is seen that for a Mach number range of $M = 0.5$–0.7 the results do not differ widely. With a further increase in M (i.e., M approaches unity), phase distortions increase sharply. For an M greater than unity, we obtain a solution

approximately equal to the results of the isobaric approximation, but two times greater. It can be shown analytically that for M approaching infinity this conclusion is correct.

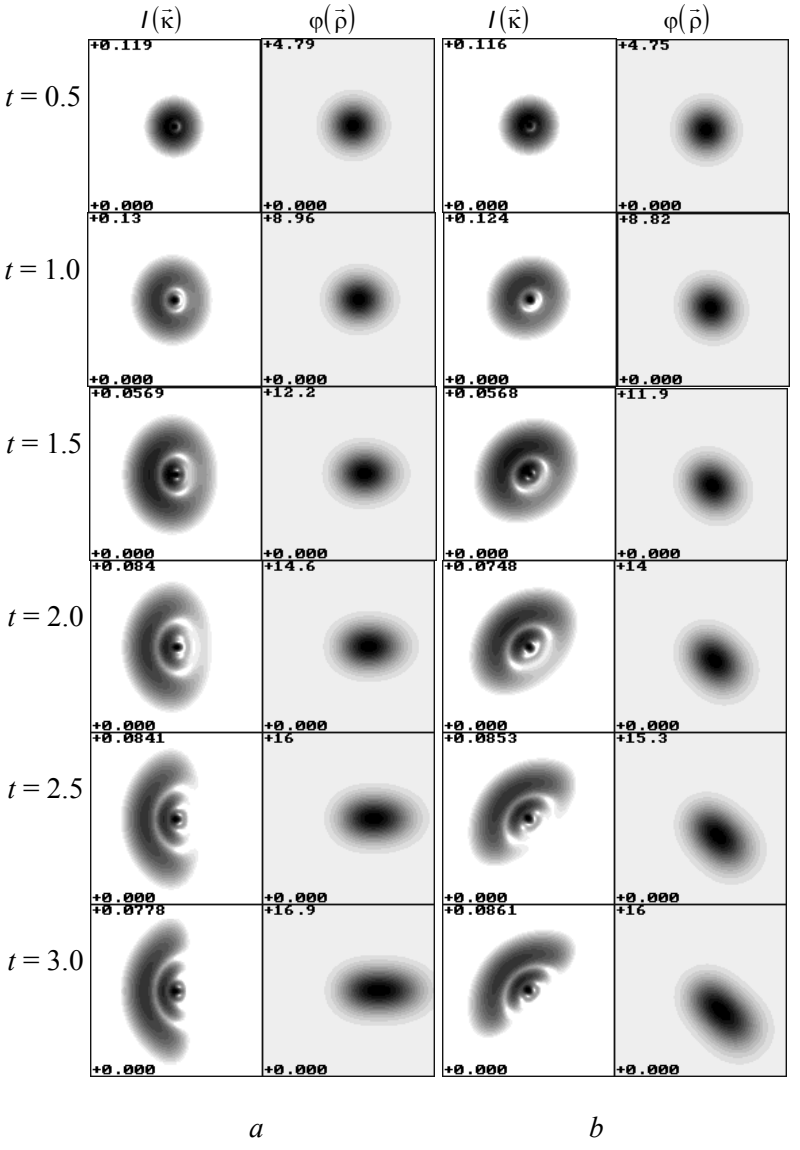

Figure 1.1.1. Dynamics of thermal blooming under conditions of forced convection (isobaric approximation): (a) wind is directed along the 0x-axis and (*b*) at an angle of 45 deg to the 0x-axis; $I(\vec{\kappa})$ is the intensity distribution in the far zone; $\varphi(\vec{\rho})$ is the phase screen.

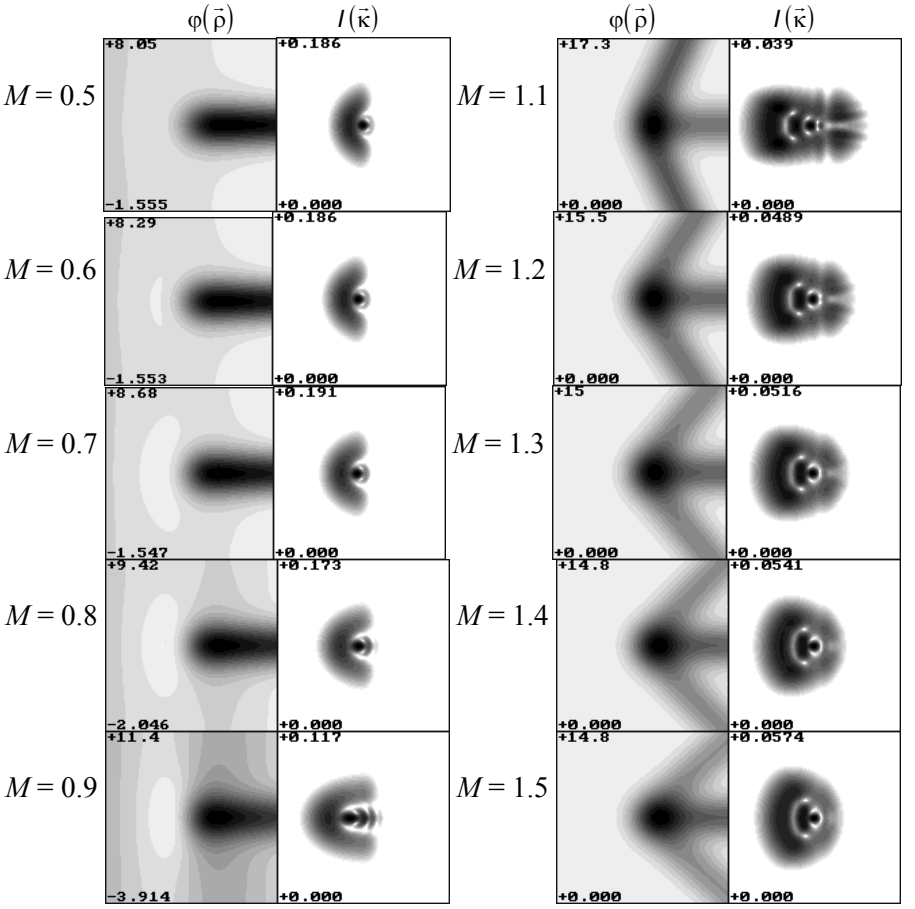

Figure 1.1.2. Thermal blooming behind the phase screen under conditions of forced convection (stationary solution of the linearized equations of hydrodynamics); $I(\vec{\kappa})$ is the intensity distribution in the far zone, $\varphi(\vec{\rho})$ is the phase screen.

1.1.3 Turbulent distortions of a wavefront

Under conditions of turbulent fluctuation, the longitudinal scale of variability of the refractive index is on the same order as the inner scale of turbulence l_0, which is usually much less than the discretization step Δz for a reasonable (in terms of computational expense) number of integration steps for the wave equation. In this case, integration of refractive index inhomogeneities along the z coordinate should be performed analytically. And, because a statistical method is used to describe turbulent fluctuations $\delta n(\vec{\rho}, z)$, the integration yields the equation for statistical characteristics, for example, the correlation function of phase fluctuations: